2015

Salt and Water Uptake in Nanocon!nement under Applied Electric Field: An Open Ensemble Monte Carlo Study

F. Moucka

D. Bratko
Virginia Commonwealth University, dbratko@vcu.edu

A. Luzar

Salt and water uptake in nanoconfinement under applied electric field: An open ensemble Monte Carlo study

Filip Moucka[a,b], Dusan Bratko[a,*], Alenka Luzar[a,*]

Department of Chemistry, Virginia Commonwealth University, Richmond, VA 23221, USA[a]

and Faculty of Science, J.E. Purkinje University, 400 96 Ústí nad Labem, Czech Republic[b]

Permeation of electrolytes in nanoporous materials is essential in many applications in energy- and materials-technologies. Wetting of apolar nanopores can be enhanced by applied electric field, attracting water and salt ions from the unperturbed electrolyte surroundings. We study absorption of water and NaCl in the pores by Expanded Grand Canonical Monte Carlo simulation. The method implements particle insertions and deletions through incremental changes in particles' coupling with the rest of the system. We determine the field-enhanced uptake of water and ions in the pores, and concomitant changes in pore thermodynamics, as functions of field strength in the pore and salt concentration in the external bath. Pressure increase, and reduction of the wetting free energy, σ, in the pore show approximately quadratic dependence on the strength of the field, however, in narrow pores we observe an additional reduction in σ as the field attracts electrolyte into the pore. Surprisingly, the effect of *bulk salinity* on σ depends on the width of the pore *and* on the field and can change qualitatively with the strength of the field. Conforming to the Gibbs adsorption isotherm, the pores in which the salt molality is enhanced relative to the bath experience a decrease in wetting free energy with rising bulk salinity and vice versa. In narrow pores, the field can change salt depletion to excess, and consequently reverse the salinity dependence of wetting free energy from an increasing to a declining function of bulk molality. Field polarity continues to play a role, leading to asymmetric wettability at opposing walls as previously observed in the absence of ions. In wide pores, salt molality can considerably exceed the solubility limit of the bulk phase, however, no precipitation is indicated during accessible simulation times in these cases.

Keywords: ionic solution, hydrophobic nanopores, electric field, wetting, regime crossover

I. Introduction

Electrolytes and polar liquids are generally attracted to field-exposed regions[1-3] due to favorable interaction associated with spontaneous polarization. A locally applied field can therefore enhance the permeation of a porous material in contact with an unperturbed electrolyte environment[4]. In macroscopic systems, the phenomenon is well understood in terms of classical electrostriction and electric double layer theories. Only molecular approaches can, however, provide accurate descriptions in nanoporous media where hydration water occupies a significant fraction of the volume of the pores[3, 5]. Molecular modeling of pore adsorption has traditionally relied on Grand Canonical Monte Carlo (GCMC) simulations[6-7]. The method was successfully applied in studies of field-driven uptake of water in laterally unrestricted confinements[5, 8-9]. In contrast to predictions from continuum theory, GCMC simulations revealed a considerable dependence of pore wettability on the direction of applied field[5]. The asymmetrical wetting, reflected in asymmetric density profiles at opposing walls, was attributed to the coupling between the orientational polarization in the field and the angular bias optimizing interfacial hydrogen bonding[5, 9]. GCMC approaches to *ionic* solutions have, however, mostly been used in conjunction with implicit (continuum) representations of the solvent[10-17]. Astronomically low acceptances of ion insertions or deletions[18-19] have so far impeded the use of direct GCMC in studies of electrolytes in the context of molecular models of water. The problem has been successfully addressed in recent studies of bulk solutions, performed in the osmotic ensemble Monte Carlo (OEMC)[20], which allows fluctuations in salt content and volume at constant amount of the solvent. The exchange of *salt* molecules was implemented in the framework of Expanded Ensemble (EE)[20-21], which introduces a new degree of freedom controlling the coupling between the exchanged ion pair and the remainder of the system. Insertions and deletions involve decoupled salt molecules, while incremental increases (or decreases) in molecular couplings

secure viable acceptances of coupling changes[20]. The simulation trajectory includes many stages in which an ion pair is partially decoupled from the rest of the system, however, statistical averages are based exclusively on fully coupled states. In the preceding study[22], the same idea was exploited in an EEGCMC Monte Carlo study of pore/electrolyte equilibria. The method enabled direct exchanges of *both*[22] the solvent (water) and solute (salt) molecules to determine their selective uptake in the pores. The study revealed a counterintuitive width dependence of salt absorption in the pores: while narrow pores (1.64 nm) showed the anticipated salt depletion (relative to bulk phase), an unexpected enrichment was observed at intermediate (2.7 nm) porevwidths[22]. As surface excess determines any change of interfacial tension, the addition of salt had opposite effects on pore wettability at different widths of the pores[22].

The present study relies on EEGCMC approach to determine the partitioning of electrolyte between the two phases under the effect of external field, and to explore the complex influence of salt ions on *electrowetting* in nanosized pores. By monitoring interfacial density profiles of water *and* ions, it answers the question about the preserved effect of field polarity[5] even in the presence of screening salt. Through calculations of solution uptake and wetting free energies, the study reaffirms a qualitative validity of classical electrostriction picture inside nanopores[3, 5], but reveals an unexpected interplay between the effects of bulk salt molality and electric field, with the salinity increasing the cost of wetting narrow pores in weak (or zero) fields while reducing it in stronger ones.

II. Methodology

Studied systems, models and methods

A. *Models.* We use classical molecular simulations to study the behavior of aqueous solutions of NaCl confined in planar hydrophobic nanopores of two different widths, h=1.64 nm and 2.7 nm.

h corresponds to the distance between the centers of the exposed surface atoms at the opposing walls of a pore; in a fully wetted pore, it exceeds the width of the liquid film by about one molecular diameter. The solutions in the nanopores are open to a bulk reservoir at pressure P=1 bar, temperature T=298.15 K, and five different values of NaCl molality m_{bulk} = 0, 1, 2, 4, 6 mol kg^{-1}. The lower width, h=1.64 nm, lies just above the kinetic threshold with respect to capillary evaporation[23-31] of water at present conditions. We model the solution using Joung and Cheatham[32-33] force fields for Na$^+$ and Cl$^-$ ions and SPC/E force field[34] for water. The ion force fields were parameterized[33] specifically for use with the SPC/E model of water. They behave reasonably well in bulk solutions over the entire experimentally accessible range of concentrations[35] and their chemical potentials are known as functions of concentration at ambient conditions[36]. They were successfully used in simulations of confined solutions[22]. SPC/E model has also been tested in aqueous confinements under external field[4-5, 8-9, 37-40].

The intermolecular interactions of these models consist of a sum of Lennard-Jones potentials for ion-ion, ion-oxygen, oxygen-oxygen pairs, and Coulombic potentials between partial charges at the centers of ions and to the interaction sites on hydrogen and oxygen atoms in water molecules. Walls of the nanopores are described by two different models. Figure 1 illustrates the simpler of these models, hereafter called smooth wall (SW) model, which describes the interaction of either wall (w) and the particle i at the position z_i by the integrated 9-3 Lennard-Jones potential[24, 41-43]

$$u_{iw}(z_i) = A_i \left(\frac{\sigma_{iw}}{|z_i - z_w|} \right)^9 - B_i \left(\frac{\sigma_{iw}}{|z_i - z_w|} \right)^3 \tag{1}$$

Above, z_w=h/2 or $-h$/2, A_i=$4\pi\rho_w\sigma_{iw}^3\varepsilon_{iw}$/45, B_i=15A_i/2, ρ_w is the presumed uniform number density of interacting sites of wall material, σ_{iw} and ε_{iw} are obtained by the Lorentz-Berthelot

rules and LJ parameters of the wall interaction sites, σ_w and ε_w. To mimic hydrocarbon walls, we

use ρ_w= 0.0333 Å^{-3}, ε_w = 0.6483 kJ mol^{-1}, σ_w = 3.742 Å. The second approach models the walls

by united-atom force fields corresponding to the structure of butylated graphane[44], a

hydrogenated derivative of graphene. Unlike graphene, the sp_3 hybridization of graphane makes
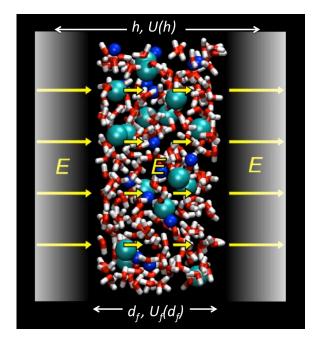

Figure 1. Model system with smooth walls (SW) at positions z_w=±$h/2$. d_f is the width of the film with nonzero simulated density of liquid atoms: oxygen (red) and hydrogen (white) from water, and Na$^+$ (magenta) and Cl$^-$ (green) ions at bulk molality 4 mol kg^{-1}. Yellow arrows denote electric field applied along z direction. The different lengths of the arrows signify the field is strongly nonuniform because of dielectric and ionic screening inside the film. U and U_f are electrostatic potential differences across the width of entire pore, h, and liquid film, d_f.

it an insulator and renders its planar structure insensitive to functionalization. The details of this

model, termed the molecular wall (MW) model, and its Lennard-Jones parameters are specified

in refs.[4, 22]. The MW model is illustrated in Figure 2. The separation between molecular walls in

MW model was adjusted to produce the thickness of the liquid film close to that observed in the

1.64 nm pore with smooth walls. Parameterization of both models[4, 24] secures contact angle Θ_c

between the SPC/E water (surface tension γ=0.063 mN/m [45]) and the modeled walls within

~127±3°.

The confinement is spanned by electric field perpendicular to the walls. In contrast to molecular simulations in homogeneous phases, where tin-foil boundary conditions[6-7] allow a direct input of the *actual* electric field strength, conventional approaches to heterogeneous systems rely on the imposition of specified electric displacement field, $D_z=E_o\varepsilon_o$, equivalent to the
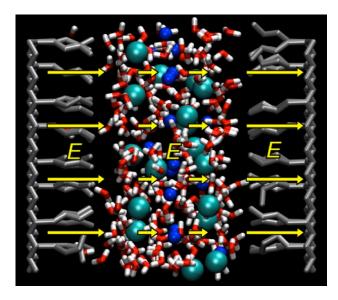

Figure 2. Model system with molecular walls comprised of butylated graphane planes in united-atom representation. Confined NaCl solution maintains equilibrium with bulk phase of molality 4 mol kg^{-1}.

charge density on the virtual capacitor electrodes outside of the nanopore (ε_o is permittivity of free space). We consider four values of D_z within the interval $0 \leq D_z \leq 0.0266$ Cm^{-2}, corresponding to hypothetical *vacuum* fields $E_o=D_z\varepsilon_o^{-1}=0$, 0.1, 0.2 or 0.3 VÅ^{-1}. This window includes displacement fields D_z above the thermodynamic threshold $D_z^c \approx \sqrt{4\gamma\cos\theta_c\varepsilon_o h^{-1}}$ (0.022 and 0.029 Cm^{-2} for h=2.7 and 1.64 nm, respectively). Fields $D_z > D_z^c$ render the liquid state in the model confinement truly stable with respect to capillary expulsion[4, 46]. Unlike the vacuum field E_o, the actual field $E(z)$ is strongly nonuniform, and significantly weakened due to dielectric and ionic screening[38, 47]. Screened field strengths $<E>$ (averaged across entire nanopore) are between 0-

0.043 VÅ^{-1} in the narrower, up to 0.029 VÅ^{-1} in the wider pores. These fields are well below the decomposition field strength E_d for water ($E_d \sim$ 0.3-0.4 VÅ^{-1}) [48-49] and close to reported fields in ion channels[38], in the vicinity of polyelectrolytes[50-52], in a micro-capacitor[53], or at the tip/solution interface in the AFM experiment[54].

B. *Methods.* We study these systems by methods described in our recent work[22]. Therefore, here we present only a brief description and refer the reader for more details to the previous paper[22]. Thermodynamic equilibrium of the solution in the nanopore is maintained using Monte Carlo simulation method in the grand canonical ensemble at the values of chemical potentials of NaCl and of water obtained by molecular simulations in osmotic ensemble[20, 36] as functions of the solution molality in the bulk reservoir, m_{bulk}. To secure viable efficiency, GCMC particle insertions/deletions are realized using expanded statistical ensemble (EEGCMC), changing particle counts gradually through a sequence of intermediate states containing fractional (partially decoupled) particles[20, 22]. These intermediate states are excluded from the resulting sequence of generated configurations used for determining the average values of calculated thermodynamic and structural properties, thus not affecting the resulting mean values. We split the process of inserting or deleting a water molecule to 5 subprocesses changing the coupling parameter λ of the fractional molecule and the process changing the amount of NaCl to 15 such subprocesses. In both these cases, this ensured acceptance probability of λ-changes around 0.4. The content of the nanopore is simulated in periodic boundary conditions in the directions parallel to the nanopore, substituting a nanopore of infinite dimensions in these directions. Electrostatic interactions are calculated by the slab-corrected Ewald method of Yeh and Berkowitz[55] where artificial interactions of the images in the direction z perpendicular to the walls are suppressed by adding a compensating energy term ($M_z^2/2\varepsilon_o V$) and inserting an empty

space of 10 nm between the images along z direction. M_z is the instantaneous z component of the net dipole of the system and V the volume of the simulation box. We use the value of the screening parameter $\alpha = \pi/R_c$, $15 \times 15 \times 19$ vectors in the reciprocal space and the cutoff value $R_c = 9.8$ Å. Long range tail corrections to the Lennard-Jones interactions are treated by a method based on a consideration that the number density is homogeneous in the directions parallel to the pore; the method is described in detail in our recent paper[22].

We focus on determining structural and thermodynamic properties of the confined solutions. We measure profiles of different properties across the nanopore: number density ρ_N, charge density ρ_q, orientation of water molecules due to the external electric field, $\cos(\theta)$, and the salt molality in the pore, m. We calculate the values of configurational energy, pressure acting on the walls of the nanopore, i.e., average pressure tensor component P_{zz}, and the pore-width average of the pressure tensor component in the directions parallel to the nanopore, $P_{xx}=P_{yy}$, with a common notation $P_{||}$. Virial terms of pressure components are calculated based on numerical differentiation of the energy with respect to the dimensions of the simulated system[5, 56-57]; details are found in our previous paper[22]. In order to verify our results, we also calculate P_{zz} directly from the average force acting on the walls; the results agree very well with those based on the numerical calculation of the virial term. We obtain free energy of wetting of confinement walls, σ, according to the relation $\sigma = - <P_{||}>h/2$, where h is the width of the pore[5]. Identical physical situations could, in principle, be described using different definitions of h, however, for all choices of h exceeding the width of the liquid film, $<P_{||}> \propto 1/h$, leaving σ independent of detailed definition of h.

In these simulations, each attempted MC move is comprised of one of the following randomly chosen MC steps:

1. λ-changing step with 10% probability. Depending on the running process either water molecule or ion pair λ-values are changed. They are either increased or decreased with equal probability. When no process is running, a new process is started, either water insertion, water deletion, ion pair insertion, ion pair deletion - all of these with equal probabilities.

2. Translation of fractional particles with 10% probability. Either fractional water or fractional ion pair is translated depending on which process is running at the instance.

3. Rotation of the fractional water molecule with 10% probability.

4. Translation of a random non-fractional particle with 35% probability.

5. Rotation of a random non-fractional particle with 34% probability.

6. Translation of all particles in the z-direction simultaneously with 1% probability.

The total number of attempted MC steps necessary to equilibrate the solution in the nanopore, starting from an initial configuration containing pure water depends on concentration in the bulk reservoir and on the width of the nanopore, from about $1 \cdot 10^9$ attempted moves for $m_{bulk} = 1$ mol kg^{-1} and the 1.64 nm pore, to about $5 \cdot 10^9$ for $m_{bulk} = 6$ mol kg^{-1} and the 2.7 nm pore. Equilibrium of the solution in the nanopore was identified by observing convergence profiles of particle counts, potential energy, pressure tensor components, voltage across the nanopore - they all exhibit reasonably flat behavior after the above equilibration lengths. The total number of MC moves attempted during the whole simulation varied from $5 \cdot 10^9$ for $m_{bulk} = 1$ mol kg^{-1} and the 1.64 nm pore, to $8 \cdot 10^9$ for $m_{bulk} = 6$ mol kg^{-1} and the 2.7 nm pore. The simulations typically ran on AMD Opteron 2.2 GHz processors using 8 cores from 5 to 14 weeks.

C. *Calculation of voltage and dielectric shielding across the nanopore.* The applied field, E_o, polarizes the liquid film in the nanopore through reorientation of water molecules and partial redistribution of ions in the pore. The actual voltage across the pore, $<U>\sim E_o h \varepsilon_{eff}^{-1}$, is significantly reduced by this polarization[38, 47]. The screening factor, ε_{eff}^{-1}, corresponds to the average of the inverse perpendicular dielectric function $<\varepsilon_\perp(z)^{-1}>_h$ across the pore[58]. Values $\varepsilon_{eff}^{-1} < O(10^{-1})$ are typical for nanoscale aqueous confinements[38-39, 47]. Calculation of the actual voltage across the pore is important for comparison with experiments where the known property is usually the voltage between electrodes at opposite sides of the pore. Alternatively, a simulation at fixed voltage between the electrodes could have been performed, however, based on implementations in Molecular Dynamics, such simulations significantly increase computing time[59-60] and are impractical in combination with the compute intense EEGCMC method. We calculate the voltage reduction $<\Delta U>=<U>-E_o h$ due to the polarization of the solution in the nanopore between the electrodes under applied field E_o. We sample $<\Delta U>$ in a Monte Carlo simulation by inserting virtual test charges to two test planes placed symmetrically outside of the screening liquid film of thickness d_f, parallel to the walls, and with their mutual distance $l > d_f$. The method is based directly on the definition of voltage, i.e., ΔU is the change of the potential energy due to the transfer of a unit charge between specified locations. Here, the test charge moves between test planes on opposite sides of the nanopore. ΔU does not contain the contribution due to the externally imposed field $-E_o l$. $<\Delta U>$ is therefore *independent* of the choice of the positions of the planes provided that the entire liquid film is between the test planes. The voltage between the virtual electrodes separated by distance l is then obtained as the sum $-E_0 l + <\Delta U>$. In order to suppress potentially large fluctuations, the value of l is chosen

sufficiently large ensuring that the charged sites from molecules in the pore do not come too close to the test planes; in the case of SW model we use l=1.64 nm or 2.7 nm, identical to the widths of the pores h. In the case of softer MW walls, which allow limited molecular penetration, we use l=2.81 nm, placing test charges well outside ~ 2nm wide region with nonzero density of water atoms. The magnitude of the test charge, in principle, plays no role. However, to optimize numerical accuracy, the magnitude should be comparable to charges typically found in the system; we use the magnitude equal to the charge of proton, e_o. We obtain $<\Delta U>$ as an average from 10 insertions of the test charges to random positions on each of the test planes for a given configuration, and these values were averaged over typically about 10^6 configurations generated during the molecular simulation.

III. Results and Discussion

A. *Structure.* Our earlier studies in similar systems in the absence of external field revealed a nonmonotonic width dependence of salt accumulation in the pores[22]. The observed behavior reflected two distinct effects: exclusion of solvated[61] ions from the 1st hydration layer next to the low-permittivity walls, and unexpected excess of ions in the core of the pores. Favorable ion-water interaction in the core is associated with orientational layering[22, 62-63] of water. This layering leads to oscillations of charge density due the imbalance of local charge densities from oxygen and hydrogen atoms (bottom part of Figures 3, 5 and 6 in ref.[22]) and ions interact favorably with a medium with inhomogeneous charge distribution[64-65]. The combined result of competing surface and core effects is depletion of ions in the narrower pore, h=1.64 nm, where the deficit of ions at the walls dominates any surplus in the core. At intermediate pore diameters, the excess of ions in the core compensates or even outweighs the depletion at the walls. The pore molality of NaCl at the bigger width, h= 2.7 nm, exceeds the molality of bulk solution. In field-

free systems, the trend toward depletion or excess depends primarily on pore width but is essentially independent of bulk concentration[22].

Under the field, the situation becomes more complicated as the field supports additional accumulation of ions in the pores. In Figure 3, we present the variations of the number of confined water and salt molecules, and the corresponding pore molalities as functions of the average field strength $<E>=<U>/h$ across the wall-to-wall distance. $<E>$ represents the average over entire separation h between wall centers including the regions close to the walls, which are
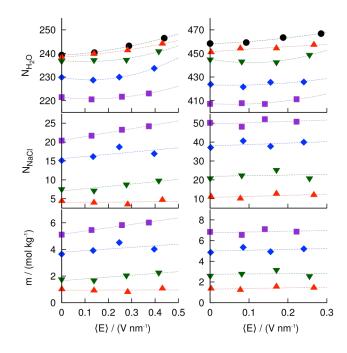

Figure 3. Number of water molecules (top), NaCl (middle) molecules, and NaCl molalities (bottom) inside a laterally replicated simulation cell of a planar pore with smooth wall separation h=1.64 nm (left) or 2.7 nm (right) as functions of the average electric field E across the cell. The lateral size of the cell L_{xy}=2.5 nm. The pore maintains equilibrium with the unperturbed reservoir containing pure water (black circles) or NaCl solutions with molalities m_{bulk}=1 mol kg^{-1} (orange triangles), 2 mol kg^{-1} (green triangles), 4 mol kg^{-1} (blue diamonds), or 6 mol kg^{-1} (purple squares) at ambient pressure and temperature. Dotted lines are quadratic fits through the points. Statistical uncertainties are of the order of $\pm$1% for N_{H_2O} and $\pm$5-10% for N_{NaCl} and confinement molalities, m. The highest wall-to-wall voltage, hE, is 0.72 V in the narrower, and 0.75 V in the wider pore.

devoid of solution molecules. The values of $<E>$, calculated in a set of prototypical systems by incorporating the screening effect of the liquid, are presented in Table 1. The average field $<E_d>=<U_d>/d_f$, averaged only over the narrower region d_f (shown in Figure 1) accessible to charged sites of the molecules in the liquid film, is 5-7 times weaker than $<E>$ (see Table 1). The observed increase in the number of water molecules with intensified field, shown in top row of Figure 3 is consistent with electrostriction effects observed at similar conditions in the absence of salt[3, 5, 8-9, 38]. The slowed increase in N_{H2O} at higher salt molalities can be attributed to steric competition between water and ions.

The *increase* in the uptake of salt molecules due to the external field should be commensurate to external charge corresponding to the applied electric displacement field D_z, $\Delta N_{NaCl} = O(D_z L_x L_y e_o^{-1})$. $L_x L_y$ is the lateral area of the simulation box. For typical box size of 2.5 nm and fields D_z considered in Table 1, this suggests $\Delta N_{NaCl}=O(1)$. The field-induced changes in N_{NaCl}, shown in Figure 3, are within the range 0-5, notwithstanding statistical uncertainties due to

Table 1. Average voltage $<U>$ between the centers of pore walls at distance h=16.4 or 27 Å, voltage drop $<U_f>$ across the width of the liquid film d_f, (the width of nonzero liquid-atom density d_f=14.5 Å in the narrower and 25.1 Å in the wider pore), average electric field spanning the entire width h, $<E>=<U>/h$, at different bulk molalities of NaCl and electric displacement fields D_z. For salt-free systems, we also list effective dielectric constants *inside* the width d_f of the liquid film, $\varepsilon_f = <\frac{1}{\varepsilon_\perp(z)}>_{d_f}^{-1}$.

D_z/Cm^{-2}	$\frac{m_{bulk}}{mol\ kg^{-1}}$	h/Å : 16.4 $\frac{<U>}{V}$	16.4 $\frac{<U_f>}{V}$	16.4 $\frac{<E>}{V\text{Å}^{-1}}$	16.4 ε_f	27.0 $\frac{<U>}{V}$	27.0 $\frac{<U_f>}{V}$	27.0 $\frac{<E>}{V\text{Å}^{-1}}$	27.0 ε_f
0.00885	0.0	0.23	0.040	0.0140	35	0.25	0.061	0.0093	42
0.0177	0.0	0.47	0.093	0.0287	30	0.52	0.127	0.0193	39
0.0266	0.0	0.70	0.150	0.0427	28	0.77	0.199	0.0285	38
0.0177	2.0	0.455	0.079	0.0277	-	0.40	0.08	0.0148	-
0.0177	4.0	0.405	(0.03)	0.0247	-	0.65	0.04	0.0241	-

the slow convergence of the EEGCMC method. Overall, the dependence of the number of confined salt molecules on the field appears stronger in narrower pores. The biggest increase in N_{H2O} within the specified range of fields $<E>$ was 2.5% (relative to the value of N_{H2O} at $E=0$), while we observe up to 25% increase in N_{NaCl}. These values correspond to the narrower pore and the highest bulk concentration, where we obtain best statistics in computed N_{NaCl}. When field is weak, salt *molality* in the narrower pore ($h=1.64$ nm) is below the bulk value, m_{bulk}, in analogy with earlier results[22] without the field. In stronger fields, pore molality increases above the bulk value. In wider pores, molalities exceed bulk values at all fields. At $m_{bulk}=6$ mol kg^{-1}, the solution is only slightly below the experimental solubility limit of ~ 6.14 mol kg^{-1} [66] and is already supersaturated with respect to the model estimates for given force fields[33-34], which are close to 4 mol kg^{-1} [67]. In this system, the molality in the wider confinement reaches around 7 ± 0.2 mol kg^{-1}, however, no precipitation transition is indicated at even the longest runs (up to $8 \cdot 10^9$) cycles, accessible to our simulation. While the lack of precipitation in the bulk phase is attributed to the activation barrier to homogeneous nucleation, the confined solution also shows partial ion demixing as ion distributions adjust to the oscillatory charge-density profile associated with the layered structure of water inside the confinement (Figures 4-6).

Figures 4, 5, and 6 compare the structures of confined liquid films maintaining equilibrium with the reservoir at bulk NaCl molalities $m_{bulk}=0$, 2 or 4 mol kg^{-1}, all at electric displacement field D=0.0177 As m^{-2}, ($E_o=D_z/\varepsilon_o=0.2$VÅ^{-1}). The actual field in the pore is nonuniform, with strong oscillations related to nonuniform screening[47, 68]. At the specified electric displacement field, the mean field strength $<E>$ averaged over the entire wall-to-wall distance was between 0.0247-0.0288 VÅ^{-1} in the narrower, and between 0.0150-0.0188 VÅ^{-1} in the wider pores. The wall-to-wall voltage $<U>$ was between 0.405 and 0.507 V in all cases

considered in Figures 4-6. Width h, spanned by voltage $\langle U \rangle$, includes the low permittivity regions outside the liquid film (film thickness $d_f < h$). As a consequence, $\langle U \rangle$ exceeds the potential drop across the film, $\langle U_f \rangle = -E_0 d_f + \langle \Delta U \rangle$, by up to an order of magnitude (Table I).

Due to the attraction of salt ions into the field-exposed pore, salt molalities in the narrower pore exceed the bulk ones by up to 10%, and about 20% in the wider pore. In analogy with field-free electrolyte systems (see Figure 6 in ref.[22]), the ions are excluded from the 1st hydration layer at the walls to preserve their hydration shells. Exclusion is especially pronounced with Na^+ ions.

Distributions of oxygen and hydrogen atoms of water (Top rows in Figs. 4-6) show pronounced layering, a feature well known[41] from studies in pure water. Although water molecules have no net charge, oxygen and hydrogen atoms carry partial charges of opposite signs, separated by the length of the O-H bond (~1Å). Water orientations next to confining walls are biased[41-42, 63] to optimize interfacial hydrogen bonding[41, 69]. We illustrate water's orientational order in terms of cosine of the angle between molecular dipoles and z axis, normal to the walls. Solid lines in middle rows of Figs. 4-6 were calculated under applied external field and dotted ones in the absence of the field. The order propagates through several molecular layers from the walls. Since molecular orientations are biased, average *local* charge densities due to oxygens and hydrogens are not entirely balanced, leading to an oscillatory charge density profile[47] (bottom rows in Figs. 4-6). The existence of this phenomenon has long been known[47] and we have recently demonstrated[22] it survives at high concentrations of salt. When salt is introduced, ions between confinement walls acquire oscillatory density profiles of their own[22, 70], with layers of Cl^- ions preferring regions with positive local charge density from water atoms, and Na^+ ions the regions with negative one[22]. By partially neutralizing local charge, salt ions
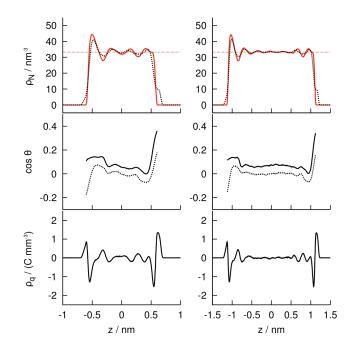
Figure 4. Top: number density profiles of oxygen atoms (red, solid lines) and half the number density of hydrogen atoms (black, dotted lines) of pure water in pores of diameter h=1.64 nm (left) or 2.7 nm (right) under average wall-to-wall voltage of 0.49±0.02V. Middle: position dependence of the (average) cosine of the angle θ between water dipoles and the direction of the field, which is perpendicular to pore walls in the presence (solid black) or absence (dotted line) of electric field. Bottom: net charge-density profile (solid black) due to uneven distribution of oxygen and hydrogen atoms.

actually enhance the orientational order of water molecules as evidenced by comparing middle rows in Figs. 5-6 (salt solutions) with those for pure water, Fig. 4.

Applied electric field destroys the symmetry of structural profiles in the pore. The density peak of water next to the left wall (with field pointing into the liquid phase) is strongly enhanced compared to its height in the absence of the field, while the peak at the r.h.s. wall (field pointing toward the solid) remains almost unaffected by the field. The confined film forms a Janus interface[3, 5], with the surface under incoming field appearing considerably more hydrophilic whereas there is no significant change in the wettability at the opposite wall. The strong dependence of interfacial properties of water, both static[3, 5, 9, 71] and dynamic[40], on the *direction* of external field has so far been studied primarily in neat water. In these works[3, 5, 9, 40, 71], the

16

discrimination with respect to field direction was explained[5] in terms of an interplay between spontaneous water orientations optimizing interfacial hydrogen bonding[41, 69] and the alignment with the external field. The spontaneous angle bias is further amplified at increased packing under the field. Orientation of water molecules around dissolved ions, however, can randomize water orientations relative to the surface, rising the question[63] if the presence of salt can blur the field-polarity dependence of wetting in water. The present results provide an unambiguous answer to this question. While the peaks increase with salt molality, the asymmetry of the oxygen density profile at $m_{bulk} = 2$ mol kg^{-1} (Figure 5) and 4 mol kg^{-1} NaCl (Figure 6) remains essentially equal as observed at otherwise identical conditions in neat water (Figure 4). Density
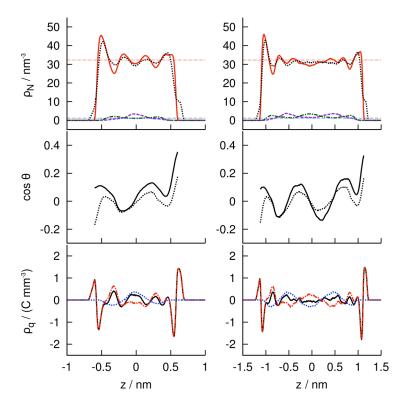

Figure 5. Top: number density profiles of oxygen atoms (red, solid lines), half the number density of hydrogen atoms (black, dotted lines), chloride (green, dot-dashed) and sodium (purple, dashed) ions in pores of diameter h=1.64 nm (left) or 2.7 nm (right) under average wall-to-wall voltage of 0.43±0.02V and bulk NaCl molality m_{bulk}=2 mol kg^{-1}. Middle: position dependence of the (average) cosine of the angle θ between water dipoles and the direction of the field, which is perpendicular to pore walls in the presence (solid black) or absence (dotted line) of electric field. Bottom: net charge-density profile (solid black) and charge densities due to water molecules (dot-dashed red), and combined charge density due to salt ions of both types (Na$^+$ and Cl$^-$, dotted blue).

profiles of the ions in Figures 5-7 show only a slight field-induced asymmetry. Small *relative* changes are explained by high absolute concentration and limited ion mobility within the structured interfacial layers of water in the nanopore.

The graphs in the 2nd row of Figures 4-6 quantify the extent of alignment of water dipoles with external field in terms of cosθ, θ being the angle between the two vectors. In pure water, the field-induced polarization observed on the l.h.s. wall cooperates with spontaneous polarization in the absence of field[69], explaining the crowding of water molecules at the l.h.s. wall (top row in Figure 4). The first adsorption layer of ions, situated approximately between the 1st and 2nd
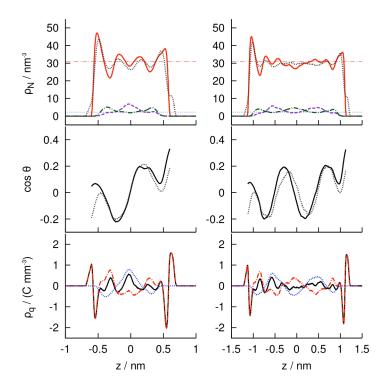

Figure 6. Top: number density profiles of oxygen atoms (red, solid lines), half the number density of hydrogen atoms (black, dotted lines), chloride (green, dot-dashed) and sodium (purple, dashed) ions in pores of diameter h=1.64 nm (left) or 2.7 nm (right) under average wall-to-wall voltage of 0.41±0.01V and bulk NaCl molality m_{bulk}=4 mol kg^{-1}. Middle: position dependence of the (average) cosine of the angle θ between water dipoles and the direction of the field, which is perpendicular to pore walls in the presence (solid black) or absence (dotted line) of electric field.Bottom: net charge-density profile (solid black) and charge densities due to water molecules (dot-dashed red), and combined charge density due to salt ions of both types (Na$^+$ and Cl$^-$, dotted blue).

hydration layers, is dominated by Cl⁻ and almost devoid on Na⁺ ions. Its negative charge gives rise to partial reorientation of water dipoles in the 2nd hydration layer by attracting partial charges on hydrogen atoms. The change is manifested in local reduction of cosθ at the position of the 2nd water peak from the l.h.s. wall, and an increase at the position of the 2nd peak from the r.h.s. wall (middle rows in Figs. 5 and 6). Spontaneous orientations of water molecules relative to the walls remain strong, giving rise to different coupling with applied electric field at opposite walls. Qualitatively similar changes are seen at both widths of the pores.

The plots shown in the bottom rows of Figures 4-6 show charge density profiles due to water (red), salt ions (blue), and the sum of both contributions (black lines). The contribution arising from water reflects not only strong packing effects but also the oscillatory orientation profile of interfacial water molecules[47, 63, 68]. The distribution of salt ions matches charge density profiles of water, with Na⁺ ions favoring the domains with the surplus of (negatively charged) oxygen atoms, and Cl⁻ ions the layers characterized by excess of hydrogen atoms. Comparison between structural profiles of confined water in the absence or presence of the electrolyte shows both situations feature strong orientational order of interfacial water. Preferred orientations of water molecules in the first hydration layer are modified in the presence of salt, however, they are not randomized, preserving the sensitivity to the *sign* of the field even at high salt concentrations. Structural properties of confined solution calculated at other field strengths and molalities, considered in Figure 3, show similar qualitative features, with field effects proportional to the strength of applied electric displacement field.

Interfacial angle bias of water dipoles is most visible on smooth or highly ordered surfaces like graphene sheets[63] or crystalline interfaces[72]. Prominent coupling between external field and spontaneous polarization of water at graphene sheets has been demonstrated in previous

works[40, 73]. Corrugations on globally flat but soft surfaces like self-assembled surfactant deposits can weaken the effect. In order to assess the role of surface undulations, in Figure 7 we present structural properties of water (left) and NaCl solution at m_{bulk}=4 mol kg^{-1} (right) confined between alkyl-functionalized graphane[44] layers. To allow comparison with coarse grained model pores considered earlier, the separation between exposed methyl groups on the opposite surfaces is set to ~16.4 Å. Because of partial flexibility of butyl functionalities, these surfaces feature spatial and temporal fluctuations around ideal planar geometry. In addition, the atomic and
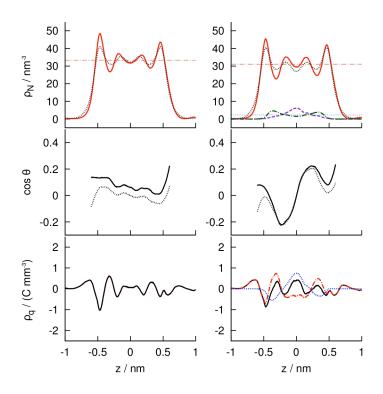

Figure 7. Top: number density profiles of oxygen atoms (red, solid lines), half the number density of hydrogen atoms (black, dotted lines), chloride (green, dot-dashed) and sodium (purple, dashed) ions in molecular-wall (MW) at conditions considered in narrow pore in Fig. 6. Left: equilibrium with a bath containing pure water , right: m_{bulk}=4 mol kg^{-1}. Middle: position dependence of the (average) cosine of the angle θ between water dipoles and the direction of the field, which is perpendicular to pore walls in the presence (solid black) or absence (dotted line) of electric field. Bottom: net charge-density profile (solid black) and charge densities due to water molecules (dot-dashed red), and combined charge density due to salt ions of both types (Na$^+$ and Cl$^-$, dotted blue).

charge density profiles in Figure 7 indicate non-negligible penetration of water molecules into the alkyl brush. Both effects broaden angular and density distributions of water molecules in the hydration layer, explaining reduced amplitudes of interfacial charge-density profiles, weaker spontaneous polarization of the surface layer, and concomitant coupling to applied electric field. Interestingly, the field continues to produce asymmetrical wetting of the opposite walls even on soft corrugated walls, although the asymmetry is smaller than on molecularly smooth walls considered in Figures 4-6. Comparison between pure water (Figure 7 left) and 4 mol kg^{-1} solution (Figure 7 right) shows a moderate reduction in propensity for wetting in concentrated salt solution, analogous to earlier observation in the absence of external field[22]. The presence of salt has, however, almost no effect on the field-induced asymmetry of the density profiles in the pore.

B. *Thermodynamics.* Is electrowetting in the pore modified by the salt? Figure 8 illustrates field dependencies of the pressure P_{zz} on the confinement walls, and wetting free energies σ of the walls as functions of the field strength <*E*> for all system conditions considered in Figure 3. Continuum level predictions for these quantities follow from expressions for Maxwell stress P_{zz} ~ ½D_z^2/ε_o,^{2} and uniform permittivity approximation for the difference between free energies[38] *per unit area* of wetted and empty pores,

$$\sigma(D_z) = \sigma(0) - \frac{D_z^2 h}{4\varepsilon_o}(1 - \frac{1}{\varepsilon_r}) \tag{2}$$

ε_r is the dielectric constant of the liquid and $\sigma(0)=\gamma\cos\Theta_c$, where γ is the surface tension of the solution. While continuum relations for the pressure increase and Lippmann-like reduction of wetting free energy retain only approximate validity in nanoscale confinement[3, 5], we confirm

roughly quadratic dependences of both P_{zz} and σ on $<E>$ at each of the fixed molalities of the

bulk phase. The impact of the field on the pressure, however, visibly increases with the molality.

The effect of the salt on the wetting free energy, is more complex because of the nonmonotonic

variation of the excess pore molality on pore width h and the strength of the field. We determine

the contribution of the salt to wetting free energy of pore walls at specified field strength $<E>$

and bulk molality, σ(m_{bulk},E), from the Gibbs adsorption isotherm[74]

$$\sigma(m_{bulk}, E) = \sigma(0, E) - \Sigma_i \int_{\mu_i(0)}^{\mu_i(m_{bulk})} \Gamma_i(\mu_i, E) \, d\mu_i \qquad (3)$$

Here, $\Gamma_i(\mu_i,E)$ denotes the excess amount of component i (water or NaCl) per unit area of the

pore at specified bulk molality and pore field E. While the sum considers both the solvent
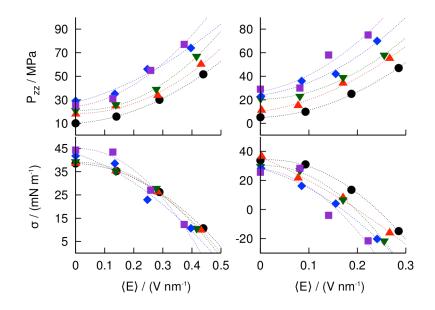

Figure 8. Top: inter-wall pressure as a function of the average field across the pores of diameter h=1.64 nm (left) or 2.7 nm (right) filled with solution in metastable liquid state. Pores are open to unperturbed bath characterized by bulk NaCl molalities m_{bulk}=0 (black circles), 1 mol kg^{-1} (red, triangles up), 2 mol kg^{-1} (green, triangles down), 4 mol kg^{-1} (blue diamonds), or 6 mol kg^{-1} (purple squares) at ambient temperature and pressure in the bulk phase. Bottom: wetting free energies at identical conditions. Error bar estimates are ± 4MPa and ±5 mNm^{-1}. Dashed lines are quadratic fits through calculated points for each molality.

(water) and solute (NaCl) contributions, the latter represents the dominant term to wetting free energy in Eq. (3). Γ_{NaCl} therefore determines the sign of the salt contribution. In the absence of applied field, salt molality is depleted in narrow pores but is increased at bigger widths[22]. Under the field, salt molality generally increases, turning the narrow pore (h=1.64 nm) salt deficit into excess at strong fields (see Figure 3, bottom left). In the wider pores (h=2.7 nm), confined molality is increased irrespective of the field. As a consequence, the wetting free energy in wider pores monotonically decreases with both the field strength *and* bulk molality of the salt. In the narrow pore, however, we observe a crossover between the weak and strong field regimes. In the weak field regime, (Γ_{NaCl} <0) σ *increases* with the molality of the bulk phase. At stronger fields, the uptake of the salt turns Γ_{NaCl} positive and σ becomes a *decreasing* function of m_{bulk}. Notwithstanding considerable statistical uncertainty, the data presented in Figure 8 clearly support this interpretation. At certain conditions, including narrow pores considered above, external field can therefore fundamentally change the role the bath salinity plays in determining the thermodynamics inside the pore. Conversely, high bulk molality (4 and 6 mol kg^{-1} in the examples considered in narrow pore systems in Figure 8) can maximize the sensitivity of pore wettability with respect to applied field inside the field-strength window corresponding to the crossover from salt-depleted to salt-enriched molalities in the confinement.

IV. *Concluding remarks*

Electrolyte absorption in porous media presents a recurring theme in electrochemistry, heterogeneous catalysis, materials, biophysical, and energy sciences. Understanding solute partitioning between the pores and surroundings has been greatly improved by insights from Grand Canonical Monte Carlo (GCMC) simulations, which offer the only rigorous simulation method to study the equilibrium between a bulk phase and laterally infinite pores. In case of

ionic solutes, the use of this method is challenging because of huge energy differences ($O(10^2)$ kT) associated with insertions or deletions of charged particles. Methodology advances are therefore essential. In the present article, we describe an application of the Expanded Ensemble GCMC[22] in a study of salt and water distribution between a bulk solution and apolar nanosized pores under external electric field. In the expanded ensemble, both ions and water molecules are exchanged by passing through a multitude of partially decoupled states; however, only states containing fully coupled particles are sampled in property calculations. The method is computationally demanding, but provides reliable insights into electrolyte phase equilibria inaccessible by standard simulation techniques.

Our calculations uncover an interesting effect of applied electric field, which can bring about a qualitative change in the salt dependence of wetting thermodynamics inside the pore. In narrow pores, which show salt depletion (compared to the bulk) in the absence of the field, this depletion can be overwhelmed by the attraction of ions through application of electric field across the pore. According to Gibbs adsorption isotherm, wettability is improved by excess solute adsorption and reduced in case of solute depletion. Increasing the field strength therefore causes a crossover from a weak-field regime where wetting free energy grows with bulk molality, to the strong-field regime characterized by a diametrically opposite concentration dependence. At field strengths corresponding to the transition between the two regimes, wetting free energy is especially sensitive to changes in applied electric field. This feature represents a departure from approximately quadratic dependence predicted by the Lippmann equation[1-2]. When the pores are wider than ~2 nm, in our systems we find the salt molality to be generally enhanced compared to the bulk. This results in a monotonic decreases in wetting free energy not

only with increasing field strength but also with *bulk* salt molality at all accessible concentrations.

Expanded Ensemble GCMC is amenable to advanced force fields including polarizable models of water and ions and tests with BK3 model[75-76] are currently in preliminary stages. The method enables applications to related problems of ion separation and ionic reaction equilibria under combined effects of confinement and electric control. These topics, along with the assessment of multi-body polarization effects, will be addressed in future studies.
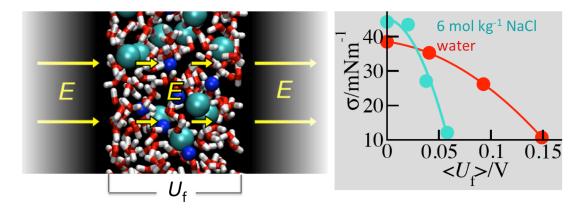
Acknowledgements

Table of contents

1.   Shapiro, B.; Moon, H.; Garrell, R. L.; Kim, C. J., Equilibrium behavior of sessile drops under surface tension, applied external fields, and material variations. *Journal Of Applied Physics* **2003,** *93* (9), 5794-5811.
2.   Mugele, F.; Baret, J. C., Electrowetting: From basics to applications. *Journal Of Physics-Condensed Matter* **2005,** *17* (28), R705-R774.
3.   Daub, C. D.; Bratko, D.; Luzar, A., Nanoscale Wetting Under Electric Field from Molecular Simulations. *Topics Curr. Chem.* **2012,** *307*, 155-180.
4.   Vanzo, D.; Bratko, D.; Luzar, A., Dynamic Control of Nanopore Wetting in Water and Saline Solutions under an Electric Field. *J. Phys. Chem. B, in press. DOI:10.1021/jp506389p, published online* **2014**.
5.   Bratko, D.; Daub, C. D.; Leung, K.; Luzar, A., Effect of field direction on electrowetting in a nanopore. *Journal of the American Chemical Society* **2007,** *129* (9), 2504-2510.
6.   Frenkel, D.; Smit, B., *Understanding molecular simulation, from algorithms to applications*. Academic: San Diego, 2002.
7.   Allen, M. P.; Tildesley, D. J., *Computer Simulation of Liquids, Clarendon, Oxford* **1987**.
8.   Bratko, D.; Daub, C. D.; Luzar, A., Field-exposed water in a nanopore: liquid or vapour? *Physical Chemistry Chemical Physics* **2008,** *10* (45), 6807-6813.
9.   Bratko, D.; Daub, C. D.; Luzar, A., Water-mediated ordering of nanoparticles in an electric field. *Faraday Discussions* **2009,** *141*, 55-66.
10.   Vlachy, V.; Haymet, A. D. J., Electrolytes in charged micropores. *Journal of the American Chemical Society* **1989,** *111* (2), 477-481.
11.   Bratko, D.; Woodward, C. E.; Luzar, A., Charge Fluctuation in Reverse Micelles. *Journal of Chemical Physics* **1991,** *95* (7), 5318-5326.
12.   Sorensen, T. S.; Sloth, P., Ion and potential distributions in charged and non-charged primitive spherical pores in equilibrium with primitive electrolyte solution calculated by grand canonical ensemble Monte Carlo simulation. Comparison with generalized Debye–Hückel and Donnan theory. *Journal of the Chemical Society-Faraday Transactions* **1992,** *88* (4), 571-589.
13.   Dzubiella, J.; Hansen, J. P., Effects of salt on the 'drying' transition and hydrophobic interaction between nano-sized spherical solutes. *Molecular Physics* **2013,** *111* (22-23), 3404-3409.
14.   Jusufi, A.; Hynninen, A.-P.; Haataja, M.; Panagiotopoulos, A. Z., Electrostatic Screening and Charge Correlation Effects in Micellization of Ionic Surfactants. *Journal of Physical Chemistry B* **2009,** *113* (18), 6314-6320.
15.   Barr, S. A.; Panagiotopoulos, A. Z., Grand-canonical Monte Carlo method for Donnan equilibria. *Physical Review E* **2012,** *86* (1).
16.   Kovacs, R.; Valisko, M.; Boda, D., Monte Carlo simulation of the electrical properties of electrolytes adsorbed in charged slit-systems. *Condensed Matter Physics* **2012,** *15* (2).
17.   Hummer, G.; Soumpasis, D. M., Correlations and free-energies in restricted primitive model descriptions of electrolytes. *Journal of Chemical Physics* **1993,** *98* (1), 581-591.
18.   Shelley, J. C.; Patey, G. N., A Configuration Bias Monte-Carlo Method for Ionic-Solutions. *Journal of Chemical Physics* **1994,** *100* (11), 8265-8270.
19.   Shelley, J. C.; Patey, G. N., Phase behavior of ionic solutions: Comparison of the primitive and explicit solvent models. *Journal of Chemical Physics* **1999,** *110* (3), 1633-1637.
20.   Moucka, F.; Lisal, M.; Skvor, J.; Jirsak, J.; Nezbeda, I.; Smith, W. R., Molecular Simulation of Aqueous Electrolyte Solubility. 2. Osmotic Ensemble Monte Carlo Methodology for Free Energy and Solubility Calculations and Application to NaCl. *Journal of Physical Chemistry B* **2011,** *115* (24), 7849-7861.
21.   Lisal, M.; Smith, W. R.; Kolafa, J., Molecular simulations of aqueous electrolyte solubility: 1. The expanded-ensemble osmotic molecular dynamics method for the solution phase. *Journal of Physical Chemistry B* **2005,** *109* (26), 12956-12965.
22.   Moucka, F.; Bratko, D.; Luzar, A., Electrolyte pore/solution partitioning by expanded grand canonical ensemble Monte Carlo simulation. *J. Chem. Phys.* **2015,** *142*, 124705.
23.   Lum, K.; Luzar, A., Pathway to surface-induced phase transition of a confined fluid. *Physical Review E* **1997,** *56* (6), R6283-R6286.
24.   Bratko, D.; Curtis, R. A.; Blanch, H. W.; Prausnitz, J. M., Interaction between hydrophobic surfaces with metastable intervening liquid. *Journal Of Chemical Physics* **2001,** *115* (8), 3873-3877.
25.   Lum, K.; Chandler, D., Phase diagram and free energies of vapor films and tubes for a confined fluid. *International Journal Of Thermophysics* **1998,** *19* (3), 845-855.
26.   Giovambattista, N.; Rossky, P. J.; Debenedetti, P. G., Effect of pressure on the phase behavior and structure of water confined between nanoscale hydrophobic and hydrophilic plates. *Physical Review E* **2006,** *73* (4), 041604.

27.   Leung, K.; Luzar, A.; Bratko, D., Dynamics of capillary drying in water. *Physical Review Letters* **2003,** *90*, 065502.

28.   Sharma, S.; Debenedetti, P. G., Free Energy Barriers to Evaporation of Water in Hydrophobic Confinement. *Journal of Physical Chemistry B* **2012,** *116* (44), 13282-13289.

29.   Leung, K.; Luzar, A., Dynamics of capillary evaporation. II. Free energy barriers. *Journal Of Chemical Physics* **2000,** *113* (14), 5845-5852.

30.   Luzar, A.; Leung, K., Dynamics of capillary evaporation. I. Effect of morphology of hydrophobic surfaces. *Journal Of Chemical Physics* **2000,** *113* (14), 5836-5844.

31.   Luzar, A., Activation barrier scaling for the spontaneous evaporation of confined water. *Journal Of Physical Chemistry B* **2004,** *108* (51), 19859-19866.

32.   Joung, I. S.; Cheatham, T. E., Determination of alkali and halide monovalent ion parameters for use in explicitly solvated biomolecular simulations. *Journal of Physical Chemistry B* **2008,** *112* (30), 9020-9041.

33.   Joung, I. S.; Cheatham, T. E., Molecular Dynamics Simulations of the Dynamic and Energetic Properties of Alkali and Halide Ions Using Water-Model-Specific Ion Parameters. *Journal of Physical Chemistry B* **2009,** *113* (40), 13279-13290.

34.   Berendsen, H. J. C.; Grigera, J. R.; Straatsma, T. P., The Missing Term In Effective Pair Potentials. *Journal Of Physical Chemistry* **1987,** *91* (24), 6269-6271.

35.   Moucka, F.; Lisal, M.; Smith, W. R., Molecular Simulation of Aqueous Electrolyte Solubility. 3. Alkali-Halide Salts and Their Mixtures in Water and in Hydrochloric Acid. *Journal of Physical Chemistry B* **2012,** *116* (18), 5468-5478.

36.   Moucka, F.; Nezbeda, I.; Smith, W. R., Molecular simulation of aqueous electrolytes: Water chemical potential results and Gibbs-Duhem equation consistency tests. *Journal of Chemical Physics* **2013,** *139* (12), 124505.

37.   Vaitheeswaran, S.; Yin, H.; Rasaiah, J. C., Water between plates in the presence of an electric field in an open system. *Journal Of Physical Chemistry B* **2005,** *109* (14), 6629-6635.

38.   Dzubiella, J.; Hansen, J. P., Electric-field-controlled water and ion permeation of a hydrophobic nanopore. *Journal Of Chemical Physics* **2005,** *122* (23), 234706.

39.   Vanzo, D.; Bratko, D.; Luzar, A., Nanoconfined water under electric field at constant chemical potential undergoes electrostriction. *Journal of Chemical Physics* **2014,** *140* (7).

40.   von Domaros, M.; Bratko, D.; Kirchner, B.; Luzar, A., Dynamics at a Janus Interface. *Journal of Physical Chemistry C* **2013,** *117* (9), 4561-4567.

41.   Lee, C. Y.; McCammon, J. A.; Rossky, P. J., The Structure Of Liquid Water At An Extended Hydrophobic Surface. *Journal Of Chemical Physics* **1984,** *80* (9), 4448-4455.

42.   Shelley, J. C.; Patey, G. N., Boundary condition effects in simulations of water confined between planar walls. *Molecular Physics* **1996,** *88* (2), 385-398.

43.   Kumar, V.; Errington, J. R., Wetting Behavior of Water near Nonpolar Surfaces. *J. Phys. Chem. C* **2013,** *117* (44), 23017-23026.

44.   Vanzo, D.; Bratko, D.; Luzar, A., Wettability of pristine and alkyl-functionalized graphane. *Journal of Chemical Physics* **2012,** *137* (3), 034707.

45.   Vega, C.; Abascal, J. L. F., Simulating water with rigid non-polarizable models: a general perspective. *Physical Chemistry Chemical Physics* **2011,** *13* (44), 19663-19688.

46.   Dzubiella, J.; Hansen, J. P., Competition of hydrophobic and Coulombic interactions between nanosized solutes. *Journal Of Chemical Physics* **2004,** *121* (11), 5514-5530.

47.   Yeh, I. C.; Berkowitz, M. L., Dielectric constant of water at high electric fields: Molecular dynamics study. *Journal Of Chemical Physics* **1999,** *110* (16), 7935-7942.

48.   Saitta, M. A.; Saija, F.; Giaquinta, P., Ab initio molecular dynamics study of dissociation of water under an electric field, . *Phys. Rev. Lett.* **2012,** *108*, 207801.

49.   Stuve, E. M., Ionization of water in interfacial electric fields: An electrochemical view. *Chemical Physics Letters* **2012,** *519-20*, 1-17.

50.   Bratko, D.; Dolar, D., Ellipsoidal Model of Poly-Electrolyte Solutions. *Journal of Chemical Physics* **1984,** *80* (11), 5782-5789.

51.   Wu, J. Z.; Bratko, D.; Prausnitz, J. M., Interaction between like-charged colloidal spheres in electrolyte solutions. *Proceedings of the National Academy of Sciences of the United States of America* **1998,** *95* (26), 15169-15172.

52.   Wagner, K.; Keyes, E.; Kephart, T. W.; Edwards, G., Analytical Debye-Huckel model for electrostatic potentials around dissolved DNA. *Biophysical Journal* **1997,** *73* (1), 21-30.

53.   Song, C. R.; Wang, P. S., High electric field effects on gigahertz dielectric properties of water measured with microwave microfluidic devices. *Review of Scientific Instruments* **2010,** *81* (5), 054702.

54.   Philippsen, A.; Im, W. P.; Engel, A.; Schirmer, T.; Roux, B.; Muller, D. J., Imaging the electrostatic potential of transmembrane channels: Atomic probe microscopy of OmpF porin. *Biophysical Journal* **2002,** *82* (3), 1667-1676.

55.   Yeh, I. C.; Berkowitz, M. L., Ewald summation for systems with slab geometry. *Journal Of Chemical Physics* **1999,** *111* (7), 3155-3162.

56.   Bratko, D.; Jonsson, B.; Wennerstrom, H., Electrical Double-Layer Interactions with Image Charges. *Chemical Physics Letters* **1986,** *128* (5-6), 449-454.

57.   Gloor, G. J.; Jackson, G.; Blas, F. J.; de Miguel, E., Test-area simulation method for the direct determination of the interfacial tension of systems with continuous or discontinuous potentials. *Journal of Chemical Physics* **2005,** *123* (13), 134703.

58.   Bonthuis, D. J.; Gekle, S.; Netz, R. R., Profile of the Static Permittivity Tensor of Water at Interfaces: Consequences for Capacitance, Hydration Interaction and Ion Adsorption. *Langmuir* **2012,** *28* (20), 7679-7694.

59.   Siepmann, J. I.; Sprik, M., Influence of surface topology and electrostatic potential on water electrode systems. *Journal Of Chemical Physics* **1995,** *102* (1), 511-524.

60.   Reed, S. K.; Lanning, O. J.; Madden, P. A., Electrochemical interface between an ionic liquid and a model metallic electrode. *Journal of Chemical Physics* **2007,** *126* (8).

61.   Rasaiah, J. C.; Lynden-Bell, R. M., Computer simulation studies of the structure and dynamics of ions and non-polar solutes in water. *Philosophical Transactions of the Royal Society of London Series a-Mathematical Physical and Engineering Sciences* **2001,** *359* (1785), 1545-1574.

62.   Sedlmeier, F.; Janecek, J.; Sendner, C.; Bocquet, L.; Netz, R. R.; Horinek, D., Water at polar and nonpolar solid walls. *Biointerphases* **2008,** *3* (3), FC23-FC39.

63.   Daub, C. D.; Bratko, D.; Luzar, A., Electric Control of Wetting by Salty Nanodrops: Molecular Dynamics Simulations. *Journal of Physical Chemistry C* **2011,** *115* (45), 22393-22399.

64.   Chakraborty, A. K.; Bratko, D.; Chandler, D., Diffusion of ionic penetrants in charged disordered media. *Journal of Chemical Physics* **1994,** *100* (2), 1528-1541.

65.   Bratko, D.; Chakraborty, A. K., Ion-ion correlations in quenched disordered media. *Journal of Chemical Physics* **1996,** *104* (19), 7700-7712.

66.   Mester, Z.; Panagiotopoulos, A. Z., Mean ionic activity coefficients in aqueous NaCl solutions from molecular dynamics simulations. *Journal of Chemical Physics* **2015,** *142* (4).

67.   Moucka, F.; Nezbeda, I.; Smith, W. R., Molecular Force Field Development for Aqueous Electrolytes: 1. Incorporating Appropriate Experimental Data and the Inadequacy of Simple Electrolyte Force Fields Based on Lennard-Jones and Point Charge Interactions with Lorentz-Berthelot Rules. *Journal of Chemical Theory and Computation* **2013,** *9* (11), 5076-5085.

68.   Ballenegger, V.; Hansen, J. P., Dielectric permittivity profiles of confined polar fluids. *Journal Of Chemical Physics* **2005,** *122* (11).

69.   Luzar, A.; Svetina, S.; Zeks, B., Consideration Of The Spontaneous Polarization Of Water At The Solid Liquid Interface. *Journal Of Chemical Physics* **1985,** *82* (11), 5146-5154.

70.   Limmer, D. T.; Willard, A. P., Nanoscale heterogeneity at the aqueous electrolyte-electrode interface. *Chemical Physics Letters* **2015,** *620*, 144-150.

71.   Daub, C. D.; Bratko, D.; Leung, K.; Luzar, A., Electrowetting at the nanoscale. *Journal of Physical Chemistry C* **2007,** *111* (2), 505-509.

72.   Ricci, M. A.; Tudisca, V.; Bruni, F.; Mancinelli, R.; Scoppola, E.; Angelini, R.; Ruzicka, B.; Soper, A. K., The structure of water near a charged crystalline surface. *Journal of Non-Crystalline Solids* **2015,** *407*, 418-422.

73.   Daub, C. D.; Bratko, D.; Ali, T.; Luzar, A., Microscopic Dynamics of the Orientation of a Hydrated Nanoparticle in an Electric Field. *Physical Review Letters* **2009,** *103*, 207801.

74.   Horinek, D.; Netz, R. R., Specific ion adsorption at hydrophobic solid surfaces. *Phys. Rev. Lett.* **2007,** *99* (22).

75.   Kiss, P. T.; Baranyai, A., A systematic development of a polarizable potential of water. *Journal of Chemical Physics* **2013,** *138* (20).

76.   Kiss, P. T.; Baranyai, A., A new polarizable force field for alkali and halide ions. *Journal of Chemical Physics* **2014,** *141* (11), 114501.